An Investigation of Ice Formation Behavior in Vertical Annular Flow

Yanin Lomchabok, Anusorn Chinsuwan* and Saranpong Chantamuang
Department of Mechanical Engineering, Faculty of Engineering, Khon Kaen University, Nai Muang, Muang, Khon Kaen, 40002, Thailand
***Corresponding Author E-mail:** anuchi@kku.ac.th
Received: May 21, 2025; **Revised:** Sep 18, 2025; **Accepted:** Sep 19, 2025

Abstract

This study investigates the ice formation behavior in an annular flow under initial flow velocities ranging from 0.20 to 0.45 m/s. The experiment was performed to validate the Computational Fluid Dynamics (CFD). The results indicate that lower flow velocities, 0.20-0.35 m/s, promote continuous ice growth leading to full the annular passage, whereas higher velocities, 0.40-0.45 m/s, suppress ice accumulation due to enhanced convective heat transfer and disruption of the mushy zone. Importantly, it was found that the ice growth rate decreases with increasing initial flow velocities. Furthermore, the correlations for predicting the ice thickness and ice growth rate with time as power functions were developed. The correlations agreed well with the simulation results. This information is very useful for design, and operating the tubular ice machines which has never found in literatures.

Keywords: Tubular ice, Annular flow, Ice formation

1. Introduction

Latent Heat Thermal Energy Storage (LHTES) systems utilize Phase Change Materials (PCMs) to absorb and release thermal energy through the phase transition process between solid and liquid states. Due to this property, PCMs have been widely applied in various industrial sectors. However, the use of PCMs often encounters several limitations, particularly the low thermal conductivity typically less than 1 W/m·K [1] which leads to poor heat transfer performance. These limitations have led many researchers to focus on developing methods to enhance heat transfer efficiency in LHTES systems.

Among these enhancement strategies, fins are one of the most widely adopted techniques for improving heat transfer performance in PCM-based thermal energy storage systems. A wide range of fin configurations has been proposed, including triangular fins [2], triplets fins [3], corrugated fins [4], helical fin [5], anchor-type fin [6], novel configuration of fins [7], V and Y shape fins [8], and continuous or discontinuous fin [9],[10].

In addition to the use of fins, various studies have investigated the effects of modifying the geometry and shape of inner tubes or the shell-and-tube arrangement to improve heat transfer efficiency. These include horizontal vs. vertical shell-and-tube latent heat storage units [11], cylindrical and conical vertical tubes [12], elliptical pipes [13], PCM placements inside shells and tubes [14], eccentric tube positions [15–17], wavy channels triple-tube [18], and star-shaped tubes [19].

Moreover, incorporating high-heat conductive materials into PCM improves the thermal propagation rate and reduces the charging/discharging time. These materials can generally be classified into three main categories. The first group includes carbon-based materials such as expanded graphite [20], carbon fiber [21], carbon nanotube [22],[23], and graphene [24]. The second group consists of ceramic-based materials [25],[26]. The third group comprises metal-based materials, which include metal foams [27],[28] and metal nanoparticles [3],[8],[29],[30].

Building on these enhancement methods, further studies have been conducted to analyze the thermal performance of thermal energy storage systems. These systems are typically categorized into three types: single-stage TES systems, cascaded TES systems utilizing multiple PCMs [31–33], and metal foam-enhanced cascaded TES systems [25], [34]. In parallel, numerous investigations have examined the effects of system design and operating conditions, including the influence of tube wall temperature [13], [35],[36], tube diameter [37],[38], mass flow rate of heat transfer fluid (HTF) [39], and inlet temperature of HTF [38–42].

Interestingly, the basic concept of phase change heat transfer in LHTES systems has also been applied to other industrial processes, with the Tubular Ice System being a prominent example. Typically, the system consists of vertically aligned tubes through which water flows downward by gravity. Simultaneously, a refrigerant (e.g., ammonia), with a temperature below the freezing point of water, flows along the outer surface of the tubes, extracting heat from the water. This results in the formation of a thin ice layer on the inner tube wall. The mechanism closely resembles the heat transfer process in LHTES systems, where thermal energy is exchanged between a heat transfer fluid (HTF) and PCM via the tube wall during the phase change process.

Although research on Tubular Ice Systems is still limited, the similarity of their operating principles to those of LHTES systems enables the use of existing LHTES studies to improve system performance.

A review of existing studies reveals that most prior research involves stationary PCM, with only the HTF in motion during the heat exchange process. These

investigations have extensively addressed techniques such as fin integration, geometry optimization, material enhancement, multi-PCM usage, and the effects of system design and operating conditions. However, there remains a clear gap in the literature regarding configurations where the PCM is in motion. While Tubular Ice Systems represent a relevant example in which both PCM and HTF flow simultaneously, this study focuses on a simplified setup in which only the PCM flows, highlighting the influence of its initial velocity and annular flow geometry on ice formation.

This research aims to address this knowledge gap by examining the ice formation behavior in a tubular ice system featuring annular flow characteristics and flowing PCM. The study specifically focuses on the effect of the PCM's initial velocity, which could significantly influence heat transfer performance and the solidification process. This knowledge provides useful guidance for designing and operating tubular ice machines, a subject that has not previously been reported in the literature.

2. Methodology

2.1 Physical Model

The physical model used in this work is shown in **Figure 1**. It consists of two vertical concentric tubes with diameters of 39 and 10 mm, and 1200 mm long. The inner tube is filled with insulation. The flow passage is the gap between the outer and inner tubes. The outer surface of the outer tube and the outer surface of the inner tube are assumed as constant temperature wall and adiabatic wall respectively.

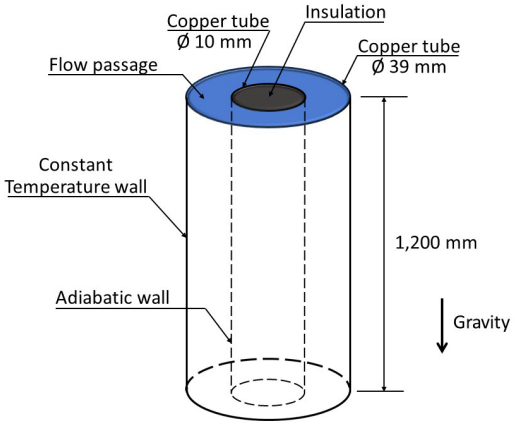

Figure 1 Schematic of the physical model.

To reduce the computational time, a two-dimensional axisymmetric model is employed in the CFD simulation. The flow direction is defined from left to right, corresponding to the gravitational direction. The tube is divided longitudinally into two regions: the entrance domain and the freezing domain. The entrance domain, 200 mm in length, is bounded by adiabatic walls, while the freezing domain, which is 1000 mm long. Uniform velocity and constant pressure at the inlet, and constant wall temperature are set as the boundary conditions. As the operating temperature at the tube surface of the most plants is -12°C, so this value is used for simulations.

In the vertical direction, the tube longitudinal-section is separated into two parts: a 5 mm-high insulation layer and a 14.5 mm-high flow region that allows PCM movement. The tube wall is considered negligibly thin and is thus excluded from the thermal calculations, as depicted in **Figure 2**.

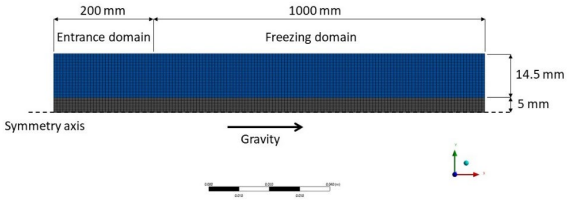

Figure 2 Computational domain.

The study investigated the effect of flow velocity on ice formation at five initial velocities: 0.20, 0.30, 0.35, 0.40, and 0.45 m/s, since experimental observations indicated that no ice formation occurred at higher velocities.

2.2 Governing Equations

To simulate the freezing behavior under annular flow conditions, the enthalpy-porosity method was employed in conjunction with a fixed computational grid. This approach allows simultaneous tracking of the heat transfer and fluid flow during phase change without explicitly tracking the moving solid-liquid interface. The assumptions made in the numerical model include transient and incompressible flow, constant thermal properties for each phase, and negligible effects of radiation and viscous dissipation.

In this research, the solidification enthalpy method was used to simulate the ice formation behavior. The total enthalpy H of the domain is defined as the sum of sensible heat and latent heat content:

$$H = h + \Delta H \tag{1}$$

where h is the sensible enthalpy and ΔH is the latent heat associated with phase change.

To model the mushy zone during solidification, the latent heat is expressed as a function of temperature:

$$\Delta H = f(T) \tag{2}$$

In the case of isothermal phase change, the function $f(T)$ is defined as:

$$f(T) = \begin{cases} L, & T < T_m \\ 0, & T > T_m \end{cases} \tag{3}$$

where L is the latent heat of fusion and T_m is the phase change temperature.

The governing equations for heat and fluid flow are as follows:

Energy equation:

$$\frac{\partial(\rho h)}{\partial t} + \nabla \cdot \left(\rho \vec{V} h\right) = \nabla \cdot (\alpha \nabla h) + S_h \quad (4)$$

where ρ is the density, $\vec{V} = (u, v)$ is the velocity vector, and α is thermal diffusivity. The energy source term is:

$$S_h = \frac{\partial(\rho \Delta H)}{\partial t} + \nabla \cdot (\rho \vec{V} \Delta H) \quad (5)$$

Continuity equation (mass conservation):

$$\frac{\partial u}{\partial x} + \frac{\partial v}{\partial y} = 0 \quad (6)$$

Momentum equations:

- x-direction:

$$\frac{\partial(\rho u)}{\partial t} + \nabla \cdot \left(\rho \vec{V} u\right) = \nabla \cdot (\mu \nabla u) - \frac{\partial P}{\partial x} + S_x + S_b \quad (7)$$

- y-direction:

$$\frac{\partial(\rho v)}{\partial t} + \nabla \cdot \left(\rho \vec{V} v\right) = \nabla \cdot (\mu \nabla u) - \frac{\partial P}{\partial y} + S_y \quad (8)$$

Here, μ is the dynamic viscosity, P is pressure, and S_x, S_y are source terms used to suppress velocity in solid regions, defined as:

$$S_x = -\frac{(1-\varepsilon)^2}{\varepsilon^3 + b} A_{mush} u \quad (9)$$

$$S_y = -\frac{(1-\varepsilon)^2}{\varepsilon^3 + b} A_{mush} v \quad (10)$$

where A_{mush} is the mushy zone constant, b is a small number (typically 0.001), and ε is the liquid fraction given by:

$$\varepsilon = \frac{\Delta H}{L} \quad (11)$$

Additionally, natural convection is modeled using a buoyancy source term S_b based on the Boussinesq approximation:

$$S_b = \frac{\rho_{ref} g \beta (h - h_{ref})}{C_p} \quad (12)$$

where β is the thermal expansion coefficient, ρ_{ref} and h_{ref} are the reference density and enthalpy, respectively, g is gravitational acceleration, and C_p is specific heat.

The equations are discretized using a second-order upwind scheme and solved using the SIMPLE algorithm within ANSYS Fluent. Convergence is achieved when the residuals for continuity, momentum, and energy equations fall below 10^{-6}.

2.3 Grid and Time Step Independence Study

To determine appropriate mesh and time-step settings for the simulation, a sensitivity analysis was performed. The rectangular grid scheme was used and the analysis involved three mesh schemes, C_1, C_2, and C_3, with total cell counts of 22,800, 46,800, and 93,600, respectively. In addition, three time-steps, $t_{s,1}$, $t_{s,2}$, and $t_{s,3}$ corresponding to 0.05 s, 0.01 s, and 0.005 s, respectively were investigated.

When the time step was fixed at 0.01 s, the change in predicted ice thickness was found to be 3.42% when the grid schemes were changed from C_1 to C_2, and 1.53% when the grid schemes were changed from C_2 to C_3. As the difference in results when the gird schemes were changed form C_2 to C_3 was minimal, C_2 was selected as the appropriate mesh resolution for further simulations.

Similarly, for grid scheme C_2, varying the time step from $t_{s,1}$ to $t_{s,2}$ and from $t_{s,2}$ to $t_{s,3}$ resulted in ice thickness differences of 2.21% and 1.96%, respectively. Given the small variation, $t_{s,2}$ (0.01 s) was deemed sufficiently accurate for time-step selection.

2.4 Experiment Setup

The experimental apparatus consists of two concentric copper tubes enclosed within a PVC pipe. The inner copper tube is fully packed with thermal insulation and acts as an adiabatic barrier, while the outer copper tube serves as the channel for water flow, forming an annular flow configuration. To induce freezing, the annular space between the outer copper tube and the PVC pipe is filled with a mixture of ice and salt (NaCl). This setup ensures a uniformly low wall temperature at the outer surface of the flow passage. The PVC pipe is further insulated with a 1-inch thick closed-cell foam to minimize heat losses. Water at an initial temperature of 0°C flows downward under gravity from a constant-level supply tank. The flow rate is regulated by a control valve located at the outlet. Temperature measurements are taken at multiple axial positions along the tube surface using T-type thermocouples. The measured wall temperatures, $T_{s,1}$, $T_{s,2}$, and $T_{s,3}$, were -10.17, -10.23, and -10.38°C, respectively. Ice thickness is measured at corresponding positions using a vernier caliper. Each test condition is repeated five times, and average values are reported. The experimental apparatus is shown in **Figure 3**. The thermocouples and data logger, vernier have accuracies of 0.1°C, and 0.02 mm, respectively. Water rotameter has an accuracy of 3%. By using the root of the sum of the square (RSS) [43], the initial velocity uncertainty can be estimated to be 3.11%.

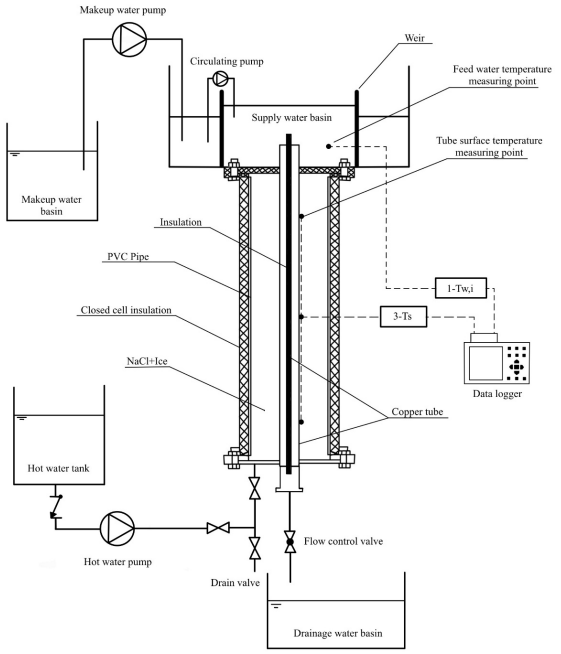

Figure 3 Experimental apparatus.

2.5 Validation

To validate the numerical model, simulation results were compared with experimental data. The simulation results closely matched the experimental data, with a maximum deviation of 1.68%, as shown in **Figure 4**. This level of accuracy was deemed acceptable for model validation purposes. Based on this comparison, a grid size of 46,800 cells and a time step of 0.01 seconds were selected for subsequent simulations. These parameters ensured numerical stability and reliable prediction of ice formation in the annular flow configuration used in this study.

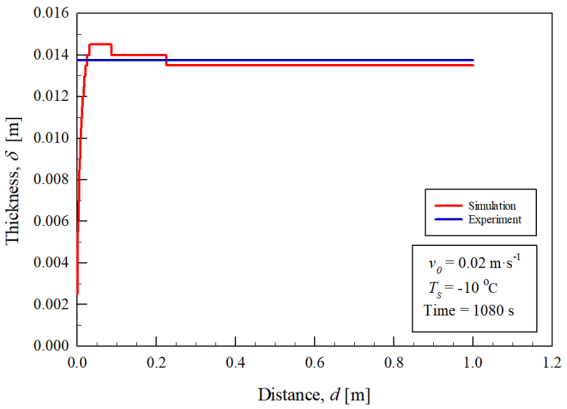

Figure 4 Comparison between experimental and simulation results.

3. Results and Discussion

Eqs. (1)–(12) were solved simultaneously by FLUENT. **Figure 5** shows the variation of ice thickness (δ) over time for different initial flow velocities ranging from 0.20 to 0.45 m/s. The ice thickness was the average measured thickness at $T_{s,1}$, $T_{s,2}$, and $T_{s,3}$. At lower velocities, 0.20, 0.30, and 0.35 m/s, the ice layer continues to grow and eventually fills the annular gap, 14.5 mm thickness. However, the growth rate decreases with increasing velocity due to enhanced convective heat transfer, which inhibits solidification.

In contrast, at higher velocities, 0.40 and 0.45 m/s, the ice growth slows significantly and does not reach 14.5 mm thickness or full the annular gap. This behavior is attributed to the disruption of the mushy zone caused by high shear forces, which prevent further solid formation.

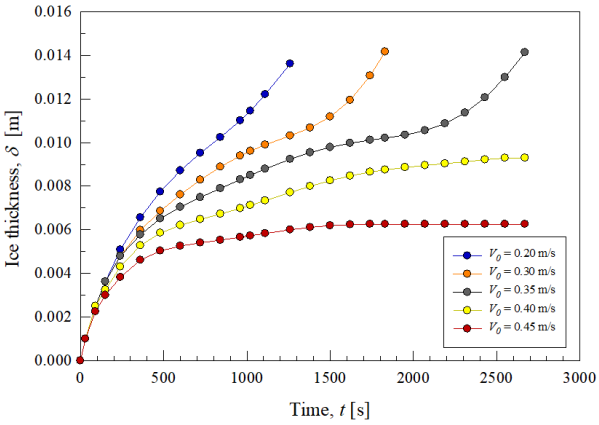

Figure 5 Ice thickness (δ) as a function of time (t) for different initial flow velocities.

Figure 6 illustrates the variation of ice growth rate (G) over time at different initial flow velocities (v_0). The ice growth rate was determined from the rate of change of ice thickness at a liquid fraction of zero. For all cases, the growth rate starts at a high value and decreases rapidly as time progresses. At lower velocities, 0.20, 0.30, and 0.35 m/s, the ice continues to grow until the annular gap is fully blocked, though the growth rate gradually diminishes.

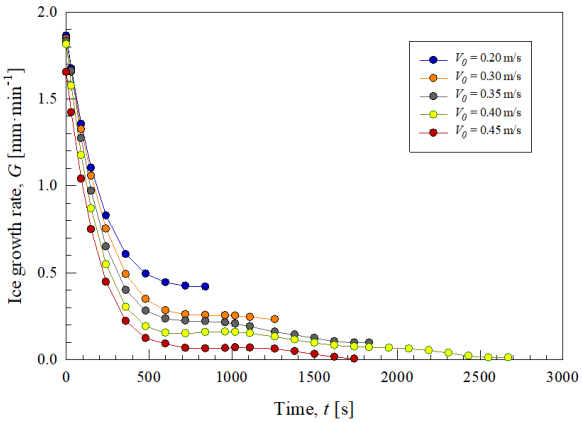

Figure 6 Ice growth rate (G) as a function of time (t) for different initial flow velocities.

In contrast, at higher velocities, 0.40 and 0.45 m/s, the growth rate drops more quickly and approaches zero earlier, indicating suppressed ice formation. This behavior aligns with the incomplete blockage observed at these velocities and reflects stronger convective effects and mushy zone disruption.

Assuming the relations between the ice thickness (δ), and ice growth rate (G) and time (t) as power functions, the relations may be written as:

$$\delta = At^m \quad (13)$$

$$G = Bt^n \quad (14)$$

where A, and B represent approximated initial ice thickness and approximated initial ice growth rate, respectively. t, m, and n are time, ice thickness rising constant, and growth rate decay constant, respectively. The regression approach is applied to the simulation results to derive the correlations, as summarized in **Table 1**.

Table 1 Summary of the correlations between ice thickness (δ), and ice growth rate (G) and time (t) for each initial flow velocity (v_0).

Parameter	Initial flow velocity [m/s]	Correlation	Coefficient of determination (R^2)
Ice thickness (δ) [m]	0.20	$\delta = 0.0001t^{0.6661}$	0.9935
	0.30	$\delta = 0.0002t^{0.5791}$	0.9834
	0.35	$\delta = 0.0003t^{0.4964}$	0.9678
	0.40	$\delta = 0.0003t^{0.4370}$	0.9623
	0.45	$\delta = 0.0005t^{0.3454}$	0.8619
Ice growth rate (G) [mm/min]	0.20	$G = 10.104t^{-0.475}$	0.9198
	0.30	$G = 18.242t^{-0.621}$	0.8883
	0.35	$G = 31.342t^{-0.747}$	0.8882
	0.40	$G = 100.30t^{-0.993}$	0.8313
	0.45	$G = 197.49t^{-1.198}$	0.7764

Based on the obtained correlations in **Table 1**, it can be observed that the coefficient A or the approximated initial ice thickness for various initial velocities are in the range of 0.0001-0.0005m which is very close to zero. Whereas, the approximated initial ice growth rate (B) increases as the initial flow velocity increases (v_0). This is due to convection heat transfer increase with the flow velocity causing higher heat transfer from the water to the tube surface. However, as time progresses, the growth rate is diminished by the mushy disruption due to the higher shear. Therefore, ice growth rate decreases as the velocity increases and hence the decay constant (n) decreases as the velocity increases.

The obtained correlations have accuracy about ±25% when they are compared with the simulation results as shown in **Figure 7**. The highest error is found at the initial stage as shown by the black solid symbols, which indicates a limitation of the power function used in this case.

4. Conclusion

This study investigated ice formation behavior in an annular flow system under various initial flow velocities. The simulation results demonstrated that lower velocities, 0.20–0.35 m/s, led to continuous ice growth and eventual the ice can be fill with the annular gap, while higher velocities, 0.40–0.45 m/s, significantly suppressed ice formation due to enhanced convective heat transfer and disruption of the mushy zone. Correlation between ice thickness, and ice growth rate and time are developed with accuracy about ±25%, except at the initial stage. This information is very useful for design, and operating the tubular ice machines which has never found in literatures.

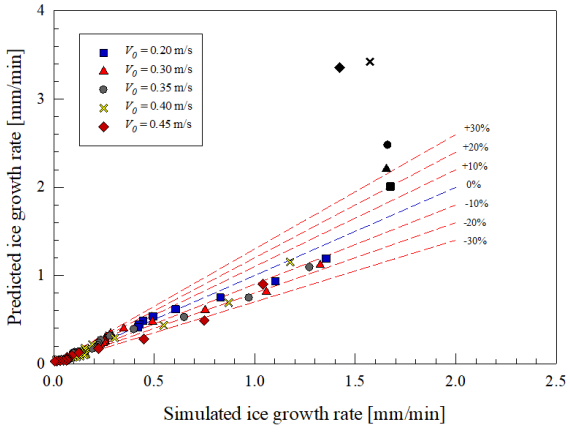

Figure 7 Comparison of predicted and simulated ice growth rate at different initial flow velocities.

5. References

[1] M. Kenisarin and K. Mahkamov, "Solar energy storage using phase change materials," *Renewable and Sustainable Energy Reviews*, vol. 11, no. 9, pp. 1913–1965, 2007, doi: 10.1016/j.rser.2006.05.005

[2] A. M. Abdulateef, J. Abdulateef, S. Mat, K. Sopian, B. Elhub and M. A. Mussa, "Experimental and numerical study of solidifying phase- change material in a triplex- tube heat exchanger with longitudinal/triangular fins," *International Communications in Heat and Mass Transfer*, vol. 90, pp. 73–84, 2018, doi: 10.1016/j.icheatmasstransfer.2017.10.003.

[3] Kh. Hosseinzadeh, E. Montazer, M. B. Shafii and A. R. D. Ganji, "Solidification enhancement in triplex thermal energy storage system via triplets fins configuration and hybrid nanoparticles," *Journal of Energy Storage*, vol. 34, 2021, Art. no. 102177, doi: 10.1016/j.est.2020.102177.

[4] K. A. Aly, A. R. El- Lathy and M. A. Fouad, "Enhancement of solidification rate of latent heat thermal energy storage using corrugated fins," *Journal of Energy Storage*, vol. 24, 2019, Art. no. 100785, doi: 10.1016/j.est.2019.100785.

[5] A. Rozenfeld, Y. Kozak, T. Rozenfeld and G. Ziskind, " Experimental demonstration, modeling and analysis of a novel latent-heat thermal energy storage unit with a helical fin," *International Journal of Heat and Mass Transfer*, vol. 110, pp. 692–709, 2017, doi: 10.1016/j.ijheatmasstransfer.2017.03.020.

[6] F. Afsharpanah, S. S. Mousavi Ajarostaghi and M. Arıcı, "Parametric study of phase change time reduction in a shell- and- tube ice storage system with anchor- type fin design," *International Communications in Heat and Mass Transfer*, vol. 137, 2022, Art. no. 106281, doi: 10.1016/j.icheat masstransfer.2022.106281.

[7] J. M. Mahdi, S. Lohrasbi, D. D. Ganji and E. C. Nsofor, " Accelerated melting of PCM in energy storage systems via novel configuration of fins in the triplex-tube heat exchanger," *International Journal of Heat and Mass Transfer*, vol. 124, pp. 663–676, 2018, doi: 10.1016/j.ijheatmasstransfer.2018.03.095.

[8] M. R. Hajizadeh, A. N. Keshteli and Q. -V. Bach, " Solidification of PCM within a tank with longitudinal-Y shape fins and CuO nanoparticle," *Journal of Molecular Liquids*, vol. 317, 2020, Art. no. 114188, doi: 10.1016/J.MOLLIQ.2020.114188.

[9] S. D. Farahani, A. D. Farahani, E. Hajian and H. F. Öztop, "Control of PCM melting process in an annular space via continuous or discontinuous fin and non- uniform magnetic field," *Journal of Energy Storage*, vol. 55, 2022, Art. no. 105410, doi: 10.1016/j.est.2022.105410.

[10] I. Sarani, S. Payan, S. A. Nada and A. Payan, " Numerical investigation of an innovative discontinuous distribution of fins for solidification rate enhancement in PCM with and without nanoparticles," *Applied Thermal Engineering*, vol. 176, 2020, Art. no. 115017, doi: 10.1016/j.applthermaleng.2020.115017.

[11] D. S. Mehta, K. Solanki, M. K. Rathod and J. Banerjee, "Thermal performance of shell and tube latent heat storage unit: Comparative assessment of horizontal and vertical orientation," *Journal of Energy Storage*, vol. 23, pp. 344–362, 2019, doi: 10.1016/j.est.2019.03.007.

[12] S. Seddegh, S. S. M. Tehrani, X. Wang, F. Cao and R. A. Taylor, " Comparison of heat transfer between cylindrical and conical vertical shell-and-tube latent heat thermal energy storage systems," *Applied Thermal Engineering*, vol. 130, pp. 1349–1362, 2018, doi: 10.1016/j.applthermaleng.2017.11.130.

[13] L. Li, H. Ma, F. Q. Si and K. P. Zhu, "Numerical Simulation on Solidification of Flow inside an Elliptical Pipe," *Applied Mechanics and Materials*, vol. 799–800, pp. 751–755, 2015, doi: 10.4028/www.scientific.net/amm.799-800.751.

[14] Y. B. Tao, Y. K. Liu and Y. L. He, "Effects of PCM arrangement and natural convection on charging and discharging performance of shell- and- tube LHS unit," *International Journal of Heat and Mass Transfer*, vol. 115, pp. 99–107, 2017, doi: 10.1016/j.ijheatmasstransfer.2017.07.098.

[15] M. R. Kadivar, M. A. Moghimi, P. Sapin and C. N. Markides, " Annulus eccentricity optimisation of a phase- change material (PCM) horizontal double- pipe thermal energy store," *Journal of Energy Storage*, vol. 26, 2019, Art. no. 101030, doi: 10.1016/j.est.2019.101030.

[16] M. S. Mahdi, H. B. Mahood, A. A. Alammar and A. A. Khadom, "Numerical investigation of PCM melting using different tube configurations in a shell and tube latent heat thermal storage unit," *Thermal Science and Engineering Progress*, vol. 25, 2021, Art. no. 101030, doi: 10.1016/j.tsep.2021.101030.

[17] J. R. Patel, M. K. Rathod and M. Sheremet, "Heat transfer augmentation of triplex type latent heat thermal energy storage using combined eccentricity and longitudinal fin," *Journal of Energy Storage*, vol. 50, 2022, Art. no. 104167, doi: 10.1016/j.est.2022.104167.

[18] A. Shahsavar, A. Shaham and P. Talebizadehsardari, "Wavy channels triple-tube LHS unit with sinusoidal variable wavelength in charging/ discharging mechanism," *International Communications in Heat and Mass Transfer*, vol. 107, pp. 93–105, 2019, doi: 10.1016/j.icheatmasstransfer.2019.05.012.

[19] Kh. Hosseinzadeh, M. A. E. Moghaddam, A. Asadi, A. R. Mogharrebi and D. D. Ganji, " Effect of internal fins along with Hybrid Nano-Particles on solid process in star shape triplex Latent Heat Thermal Energy Storage System by numerical simulation," *Renewable Energy*, vol. 154, pp. 497–507, 2020, doi: 10.1016/j.renene.2020.03.054.

[20] X. Xiao, P. Zhang and M. Li, "Experimental and numerical study of heat transfer performance of nitrate/ expanded graphite composite PCM for solar energy storage," *Energy Conversion and Management*, vol. 105, pp. 272–284, 2015, doi: 10.1016/j.enconman.2015.07.074.

[21] X. Huang, G. Alva, L. Liu and G. Fang, "Microstructure and thermal properties of cetyl alcohol/ high density polyethylene composite phase change materials with carbon fiber as shape- stabilized thermal storage materials," *Applied Energy*, vol. 200, pp. 19–27, 2017, doi: 10.1016/j.apenergy.2017.05.074.

[22] S. A. Khan, H. E. Abdellatif, A. Belaadi, A. Arshad and H. Liu, "Numerical study of shell and tube thermal energy storage system: Enhancing solidification performance with single- walled carbon nanotubes in phase change material," *International Communications in Heat and Mass Transfer*, vol. 160, 2025, Art. no. 108338, doi: 10.1016/j.icheatmasstransfer.2024.108338.

[23] T. Qian, J. Li, W. Feng and H. Nian, "Single-walled carbon nanotube for shape stabilization and enhanced phase change heat transfer of polyethylene glycol phase change material," *Energy Conversion and Management*, vol. 143, pp. 96–108, 2017, doi: 10.1016/j.enconman.2017.03.065.

[24] R. M. Saeed, J. P. Schlegel, C. Castano and R. Sawafta, " Preparation and enhanced thermal performance of novel (solid to gel) form- stable eutectic PCM modified by nano- graphene platelets," *Journal of Energy Storage*, vol. 15, pp. 91–102, 2018, doi: 10.1016/j.est.2017.11.003.

[25] J. M. Mahdi, H. I. Mohammed, E. T. Hashim, P. Talebizadehsardari and E. C. Nsofor, "Solidification enhancement with multiple PCMs, cascaded metal foam and nanoparticles in the shell- and- tube energy storage system," *Applied Energy*, vol. 257, 2020, Art. no. 113993, doi: 10.1016/j.apenergy.2019.113993.

[26] Y. Xu, Q. Ren, Z. J. Zheng and Y. L. He, " Evaluation and optimization of melting performance for a latent heat thermal energy storage unit partially filled with porous media," *Applied Energy*, vol. 193, pp. 84–95, 2017, doi: 10.1016/j.apenergy.2017.02.019.

[27] Z. Liu, Y. Yao and H. Wu, "Numerical modeling for solid- liquid phase change phenomena in porous media: Shell-and-tube type latent heat thermal energy storage," *Applied Energy*, vol. 112, pp. 1222–1232, 2013, doi: 10.1016/j.apenergy.2013.02.022.

[28] G. Righetti, C. Zilio, G. A. Longo, K. Hooman and S. Mancin, "Experimental study on the effect of metal foams pore size in a phase change material based thermal energy storage tube," *Applied Thermal Engineering*, vol. 217, 2022, Art. no. 119163, doi: 10.1016/j.applthermaleng.2022.119163.

[29] S. Tiari, M. Mahdavi, V. Thakore and S. Joseph, " Thermal Analysis of a High- Temperature Heat Pipe-Assisted Thermal Energy Storage System With Nano-Enhanced Phase Change Material," in *ASME 2018 International Mechanical Engineering Congress and Exposition*, Pittsburgh, PA, USA, Nov. 9–15, 2018, Paper IMECE2018-86481, doi: 10.1115/IMECE2018-86481

[30] N. Gupta, Am. Kumar, H. Dhasmana, V. Kumar, Av. Kumar, P. Shukla, A. Verma, G. V. Nutan, S. K. Dhawan and V. K. Jain, " Enhanced thermophysical properties of Metal oxide nanoparticles embedded magnesium nitrate hexahydrate based nanocomposite for thermal energy storage applications," *Journal of Energy Storage*, vol. 32, 2020, Art. no. 101773, doi: 10.1016/j.est.2020.101773.

[31] L. N. N. , " Assessment of latent heat thermal storage systems operating with multiple phase change materials," 2019, *Journal of Energy Storage*, vol. 23, pp. 442–455, 2019, doi: 10.1016/j.est.2019.04.008.

[32] T. K. Aldoss and M. M. Rahman, "Comparison between the single-PCM and multi-PCM thermal energy storage design," *Energy Conversion and Management*, vol. 83, pp. 79–87, 2014, doi: 10.1016/j.enconman.2014.03.047.

[33] X. Cheng and X. Zhai, " Thermal performance analysis and optimization of a cascaded packed bed cool thermal energy storage unit using multiple phase change materials," *Applied Energy*, vol. 215, pp. 566–576, 2018, doi: 10.1016/j.apenergy.2018.02.053.

[34] Y. Tian and C. Y. Zhao, " Thermal and exergetic analysis of Metal Foam-enhanced Cascaded Thermal Energy Storage (MF-CTES)," *International Journal of Heat and Mass Transfer*, vol. 58, no. 1–2, pp. 86–96, 2013, doi: 10. 1016/ j. ijheatmasstransfer. 2012. 11.034.

[35] C. R. E. S. Nóbrega, K. A. R. Ismail and F. A. M. Lino, " Solidification around axial finned tube submersed in PCM: Modeling and experiments," *Journal of Energy Storage*, vol. 29, 2020, Art. no. 101438, doi: 10.1016/j.est.2020.101438.

[36] M. Mahdaoui, T. Kousksou, J. M. Marín, T. El Rhafiki and Y. Zeraouli, " Laminar flow in circular tube with internal solidification of a binary mixture," *Energy*, vol. 78, pp. 713–719, 2014, doi: 10.1016/j.energy.2014.10.062.

[37] K. Pakzad, S. S. Mousavi Ajarostaghi and K. Sedighi, "Numerical simulation of solidification process in an ice- on- coil ice storage system with serpentine tubes," *SN Applied Sciences*, vol. 1, no. 10, 2019, Art. no. 1258, doi: 10. 1007/ s42452-019-1316-4.

[38] M. A. Kibria, M. R. Anisur, M. H. Mahfuz, R. Saidur and I. H. S. C. Metselaar, "Numerical and experimental investigation of heat transfer in a

shell and tube thermal energy storage system," *International Communications in Heat and Mass Transfer*, vol. 53, pp. 71–78, 2014, doi: 10.1016/j.icheatmasstransfer.2014.02.023.

[39] M. K. Rathod and J. Banerjee, "Thermal performance enhancement of shell and tube Latent Heat Storage Unit using longitudinal fins," *Applied Thermal Engineering*, vol. 75, pp. 1084–1092, 2015, doi: 10.1016/j.applthermaleng.2014.10.074.

[40] K. A. R. Ismail, F. A. M. Lino, R. C. R. Da Silva, A. B. De Jesus and L. C. Paixão, "Experimentally validated two dimensional numerical model for the solidification of PCM along a horizontal long tube," *International Journal of Thermal Sciences*, vol. 75, pp. 184–193, 2014, doi: 10. 1016/ j. ijthermalsci. 2013.08.008.

[41] M. Avci and M. Y. Yazici, "Experimental study of thermal energy storage characteristics of a paraffin in a horizontal tube- in- shell storage unit," *Energy Conversion and Management*, vol. 73, pp. 271–277, 2013, doi: 10.1016/j.enconman.2013.04.030.

[42] M. J. Hosseini, M. Rahimi and R. Bahrampoury, "Experimental and computational evolution of a shell and tube heat exchanger as a PCM thermal storage system," *International Communications in Heat and Mass Transfer*, vol. 50, pp. 128–136, 2014, doi: 10.1016/j.icheatmasstransfer.2013.11.008.

[43] A. J. Wheeler and A. R. Ganji, *"*Experimental Uncertainty Analysis*," in Introduction to Engineering Experimentation*, 3 rd ed. New Jersey, NJ, USA: Pearson Prentice Hall, 2004, ch. 7, sec. 7.2, pp. 199–202.